BNL-107639-2015-JA

A Review of Iron and Cobalt Porphyrins, Phthalocyanines, and Related Complexes for Electrochemical and Photochemical Reduction of Carbon Dioxide

Gerald F. Manbeck* and Etsuko Fujita*

Chemistry Department, Brookhaven National Laboratory, Upton, NY 11973, United States

Received date (to be automatically inserted after your manuscript is submitted)
Accepted date (to be automatically inserted after your manuscript is accepted)

ABSTRACT: This review summarizes research on the electrochemical and photochemical reduction of CO_2 using a variety of iron and cobalt porphyrins, phthalocyanines, and related complexes. Metalloporphyrins and metallophthalocyanines are visible light absorbers with extremely large extinction coefficients. However, yields of photochemically-generated active catalysts for CO_2 reduction are typically low owing to the requirement of a second photoinduced electron. This requirement is not relevant to the case of electrochemical CO_2 reduction. Recent progress on efficient and stable electrochemical systems includes the use of FeTPP catalysts that have prepositioned phenyl OH groups in their second coordination spheres. This has led to remarkable progress in carrying out coupled proton-electron transfer reactions for CO_2 reduction. Such ground-breaking research has to be continued in order to produce renewable fuels in an economically feasible manner.

KEYWORDS: CO_2 reduction, porphyrin, phthalocyanine, cobalt, iron

*Correspondence to: gmanbeck@bnl.gov, fujita@bnl.gov

I. INTRODUCTION

The global carbon cycle is a closed system with all fossil fuels currently burned originating from photosynthetic carbon dioxide fixation over millions of years. An imbalance in the rates of consumption vs. natural fixation with increasing human demand for energy leads to two major concerns: the rising concentration of atmospheric CO_2, and the inevitable decline of extractable fossil fuels. The problem of atmospheric concentrations can be alleviated to some extent through CO_2 capture / sequestration technology [1]; however, a conversion / utilization or recycling scheme is perhaps more ideal since the need for energy is also addressed. If the recycling technology is ultimately powered by inexhaustible, although intermittent, solar energy, CO_2 is then viewed as a redox mediator in which diffuse solar energy is stored in the form of chemical bonds by its reduction and electrical energy is obtained by oxidation of the reduced products.

The foremost challenge to CO_2 recycling is its chemically inert nature. Direct electrochemical reduction to $CO_2^{\bullet-}$ (eq 1) is highly unfavorable due in part to the geometric rearrangement from linear to bent. This difficulty is reflected by the standard potential of −1.90 V vs. NHE [2]. Energy requirements for proton assisted multi-electron reductions at pH 7 (eqs. 2 – 6) are substantially lower; however, catalysts are necessary to mediate the microscopic steps involved in the multi-proton, multi-electron reductions. Transition metal complexes with a variety of accessible oxidations states (including ligand-localized reductions) are well suited for this task and often provide product selectivity and tunable activity [3-5]. Nevertheless, reduction beyond formic acid or CO remains rare and further developments are needed.

$$CO_2 + e^- \rightarrow CO_2^{\bullet-} \qquad E^{\circ\prime} = -1.90\ \text{V} \quad (1)$$

$$CO_2 + 2H^+ + 2e^- \rightarrow CO + H_2O \qquad E^{\circ\prime} = -0.53\ \text{V} \quad (2)$$

$$CO_2 + 2H^+ + 2e^- \rightarrow HCO_2H \qquad E^{\circ\prime} = -0.61\ \text{V} \quad (3)$$

$$CO_2 + 4H^+ + 4e^- \rightarrow HCHO \qquad E^{\circ\prime} = -0.48\ \text{V} \quad (4)$$

$$CO_2 + 6H^+ + 6e^- \rightarrow CH_3OH + H_2O \qquad E^{\circ\prime} = -0.38\ \text{V} \quad (5)$$

$$CO_2 + 8H^+ + 8e^- \rightarrow CH_4 + H_2O \qquad E^{\circ\prime} = -0.24\ \text{V} \quad (6)$$

The conversion and utilization of carbon dioxide is an area of intense current research interest, and several recent review articles [6-12] provide a broader scope and overview than is possible in this Minireview. We have limited the scope of this review to articles pertaining to catalytic CO_2 reduction using iron and cobalt porphyrins, phthalocyanines, and related complexes (Chart 1). The Fe and Co centers exist from the +3 to 0 oxidation states while the macrocyclic ligand framework provides chemical stability and storage of a reducing equivalent and/or a proton. Characteristic electronic absorption spectra provide a probe into oxidation states and reaction kinetics, and mechanisms or structure-activity relationships are deciphered through the large variability in available ligands.

In this review, the papers discussed are separated into heterogeneous and homogeneous catalysis. The heterogeneous experiments employ complexes adsorbed onto or covalently bound to electrode surfaces. This technique can enhance efficiency by eliminating diffusion and mass transport, which are inevitable in solution

electrocatalysis. Catalysis in media in which the compound is poorly soluble (usually water) is then possible. The surface modification should not impede conductivity, block catalytic sites, or decrease catalyst reactivity. Two common methods of surface confinement are non-covalent adsorption and covalent anchoring to a surface through axial ligands, usually through pyridine or other monodentate ligands. The stability of an axial pyridine linkage could be problematic considering the known dissociative reactions of monodentate nitrogen ligands from $Co^{II}TPP$ upon reduction in polar solvents [13]. Conversely, ligand based reductions of $[Co(pTMPyP)]^{3+}$ trigger the coordination of pyridine to the Co center [14]. It is likely that high local concentrations of linker ligands on the electrode along with complex insolubility contribute to stabilization of catalysts covalently bound to electrodes through axial ligands.

The discussion of homogeneous catalysis is separated into purely electrochemical systems, in which cyclic voltammetry (CV) and bulk electrolysis are the primary analytical techniques, and photocatalysis, in which photochemistry, radiolysis, and chemical reduction in conjunction with visible spectroscopy identify species that react with CO_2 and provide rate constants for relevant reactions.

In all examples, we include practical parameters such as methods of electrode preparation and catalyst loading, while we highlight issues of scientific merit including Faradaic efficiency (FE), product distribution, turnovers, and kinetics. One consistently controversial issue is the nature of the active catalyst. This is especially problematic for surface bound catalysts with low loading relative to the electrode surface because of the inability to view characteristic redox couples of the catalyst. Deposition of metal colloids should always be considered, though in many cases it is not even discussed despite the occasional preparation of electrodes under harsh conditions (e.g., high temperature and pressure). Chart 1 contains most of the porphyrin and phthalocyanine ligands used for Fe and Co catalyzed CO_2 reduction. The structures of a few special cases will appear later.

Chart 1. Porphyrins and Phthalocyanines studied as CO_2 reduction catalysts.

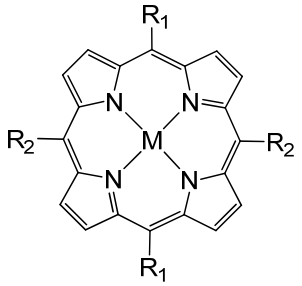

R1 = R2 = C_6H_5 MTPP
R1 = R2 = $C_6H_4(4\text{-}SO_3^-)$ MTPPS
R1 = R2 = $C_6H_4(4\text{-}CO_2^-)$ MTCPP
R1 = R2 = $C_5H_4(4\text{-}N^+\text{-}CH_3)$ M-pTMPyP
R1 = R2 = $C_5H_4(3\text{-}N^+\text{-}CH_3)$ M-mTMPyP
R1 = R2 = $C_5H_4(2\text{-}N^+\text{-}CH_3)$ M-oTMPyP
R1 = R2 = $C_6H_4(4\text{-}OCH_3)$ MTMeOPP
R1 = R2 = $C_6H_3(2,6\text{-}Cl)$ MTClPP
R1 = R2 = $C_6H_3(2,6\text{-}OCH_3)$ MTDMPP
R1 = R2 = $C_6H_3(2,6\text{-}OH)$ MTDHPP
R1 = $C_6H_3(2,6\text{-}OCH_3)$ R2 = C_6F_5 $MTDHPPF_{10}$
R1 = R2 = $C_6H_2(2,4,6\text{-}CH_3)$ MTMP
R1 = R2 = C_6H_5 + 2H (chlorin) MTPC
R1 = R2 = H MPor
R1 = R2 = $C_6H_4(4\text{-}NH_2)$ MTAPP
R1 = R2 = $C_6H_4(4\text{-}N^+(CH_3))$ MTNMPP
R1 = R2 = C_6F_5 MTPFPP
R1 = R2 = $C_6H_4(3\text{-}F)$ MT3FPP
R1 = R2 = $C_6H_4(3\text{-}CF_3)$ $MT3CF_3PP$
R1 = R2 = $C_6H_4(3\text{-}CH_3)$ $MT3CH_3PP$
R1 = R2 = H $(2,3,7,8,12,13,17,18\text{-}CH_2CH_3)$ MOEP

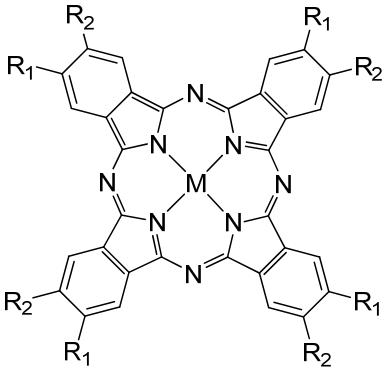

R1 = R2 = H MPc
R1 = H R2 = SO_3^- MTSPc
R1 = R2 = CN $MPc(CN)_8$
R1 = H R2 = ^{t}Bu MTBPc
R1 = H R2 = NH_2 MTAPc
R1 = R2 = $C_6H_4(4\text{-}SO_3^-)$ MTPPS
R1 = R2 = OBu $MPc(OBu)_8$
R1 = R2 = Benzo MNc

II. HETEROGENEOUS CATALYSIS

A. Catalysts Adsorbed onto Electrodes

Non-covalent adsorption is the simplest method of electrode modification. In this discussion, we use "dip coated" to describe electrodes prepared by soaking in a solution of the catalyst (usually in organic solvent) for a given time followed by drying. "Drop coating" refers to electrodes prepared by dropping a concentrated solution onto the surface and evaporating the organic solvent. The catalyst loading is usually easier to determine using the drop coating method although integration of CV current or dissolution followed by concentration determination can be used in any case. Catalyst evaluation is most easily performed by cyclic voltammetry (CV) in CO_2-saturated solvent and comparison to the current without CO_2. Relevant data are summarized in Table 1.

In early work in 1974, CoPc adsorbed on graphite was studied in a CO_2-saturated aqueous solution. The voltammogram exhibited a peak at *ca.* −1.6 V vs. SCE, which was about 200 mV more positive than the proton reduction reaction under N_2 [15]. A control scan in 0.1 M Na_2CO_3 or $NaHCO_3$ solution showed no current in the

absence of CO_2 indicating that dissolved CO_2 is reduced. When a quaternary ammonium salt was used for the electrolyte under CO_2 (i.e., pH ~4.5), oxalate and glycolate were detected by color reactions of thiobarbituric acid and 2,7-dihydronaphthalene (Table 1 entry 1). No formate was detected as a CO_2 reduction product in this early paper. In contrast, an electrode prepared by precipitation of CoPc onto glassy carbon produced formate with 60% FE during continuous electrolysis at 1 $mA.cm^{-2}$ for 72 h with 10 $\mu g.cm^{-2}$ loading (Table 1 entry 2) [16]. The CV was stable for several cycles if the switching of the potential remained positive of −1.55 V, otherwise activity was reduced to that of bare carbon. In both cases (CoPc on graphite or glassy carbon), the current was proportional to $[CO_2]$ and $\nu^{1/2}$, consistent with a diffusion controlled process whereas the peak height of a redox couple immobilized on an electrode should be proportional to ν (scan rate). On glassy carbon, the Tafel slope of ~120 mV/decade indicated that transfer of the first electron to CO_2 was the rate-limiting step.

Carbon monoxide was reported as yet another product of electrocatalysis using CoPc. In this case, the catalyst was adsorbed onto pyrolytic graphite or carbon cloth by dip coating or drop coating from THF [17]. Electrolysis experiments from −0.95 to −1.2 V vs. SCE (pH 5, citrate buffer) produced CO and H_2 (1.5:1) with 55 − 65% FE for CO and 3.7×10^5 turnovers (entry 3) at an overpotential of 300 mV. Trace amounts of oxalate and formate were detected. A control experiment with 3 mM $Co(ClO_4)_2$ yielded only 0.14 turnovers of products implicating the intact complex as the active catalyst. In solution, the CoPc was unstable to prolonged electrolysis due to hydrogenation of the Pc ligand, but deactivation was minimized on the electrode surfaces. The mechanism was investigated by CV experiments. First, binding of CO_2 to the one-electron-reduced species, $[CoPc]^-$, was ruled out since there was no change in the first redox couple under N_2 or CO_2. Aqueous CVs under N_2 showed two proton-coupled reductions, implying protonation of $[CoPc]^-$ followed by further reduction and reaction with CO_2. Additional support for this mechanism was obtained in an *in-situ* FTIR study during electroreduction of CO_2 by CoPc-coated graphite electrodes [18]. The results indicate that (1) the first reduction of CoPc occurs on the Pc ligand to produce $[Co^{II}(Pc^{\bullet-})]^-$; (2) the second reduction produced $[Co(H)(Pc^{\bullet-})]^-$ via protonation of $[Co^{I}(Pc^{\bullet-})]^{2-}$; (3) neither free nor adsorbed CO on the electrode were detected due to the relatively short-term spectroelectrochemical experiments; and (4) CO_2 reacted irreversibly with the doubly-reduced species by formation of products. The surface properties were related to electrode preparation as H_2 was generated from a film prepared from THF but not from pyridine. The assignment of the first reduction product as $[Co^{II}(Pc^{\bullet-})]^-$, is controversial as seen below.

The activity and stability of a CoPc film on glassy carbon was impacted by the method of preparation. By using vacuum deposition with intermittent plasma assistance, A uniform 40 nm film of CoPc on glassy carbon was prepared [19]. The CV showed one major peak at *ca.* −1.6 V vs. SSCE with stable current for multiple scans. In contrast, a film produced by traditional vacuum deposition showed two peaks which decreased after polarization at −1.85 V. The reduction of CO_2 seems to be controlled by a surface chemical reaction involving adsorbed H^+ and/or H and carbon-containing surface intermediates, but products of reduction were not determined.

Ligand effects were explored using $CoPc(OBu)_8$ or $CoPc(CN)_8$. A film of $CoPc(OBu)_8$ (1.2×10^{-10} $mol.cm^{-2}$) was prepared by drop casting onto a basal-plane pyrolytic graphite electrode from DMF [20]. The first reduction couple was observed at −0.58 V vs. Ag/AgCl but the second reduction was obscured by proton reduction. Interestingly, assignments of the first and second reduction couples are $Co^{II/I}$ and a ligand reaction, respectively,

which is inconsistent with a previous report on CoPc [18]. At mild potentials where H^+ reduction does not dominate the CV response, the $CoPc(OBu)_8$ modified electrode greatly outperformed CoPc with turnover frequencies of $1.1 \times 10^6\ h^{-1}$ vs. $5.5 \times 10^4\ h^{-1}$ for CO_2 reduction (entry 5). Spectral changes during electrolysis of a homogeneous pyridine solution showed stepwise $Co^{II/I}$ and $Pc^{0/-}$ reduction under N_2 while the doubly-reduced species could not be detected under CO_2. A mechanism was proposed in which the doubly-reduced, protonated species reacts with CO_2 and CO release is triggered by reduction of the putative Co(II)–COOH species. $CoPc(CN)_8$ was active for CO_2 reduction to CO at −1.20 V vs. Ag/AgCl at pH 10. In this case the ratio of CO to H_2 was 10 whereas it was 4.2 for $CoPc(OBu)_8$ (pH 6.8) [21].

Gas diffusion electrodes (GDE) [22] impregnated with CoPc were prepared by precipitation of CoPc onto carbon black from sulfuric acid. Polytetrafluoroethylene (PTFE) was added, and the paste was spread onto lead-plated nickel gauze, cured at 300 C and compressed at 10^5 kPa [23]. CO was the only carbon product of reduction (entry 6) and its partial current density was independent of applied potential; however, H_2 production increased with increasingly negative potentials. Similar experiments with Mn, Cu or Zn phthalocyanine produced varying amounts of formate suggesting differing mechanisms dependent on the metal ion. One trend is that Mn, Cu, and Zn Pc are first reduced at the ligand while CoPc first undergoes a $Co^{II/I}$ reduction. The proposed mechanism entailed reaction of CO_2 with Co(I) followed by protonation and a second electron transfer in contrast to the mechanism proposed above for $CoPc(OBu)_8$ in which the doubly reduced species is first protonated and then reacts with CO_2. Examination of GDEs with 17 different MPc showed 100% FE for CO with Co (entries 7 and 8) and Ni, while others produced formate or methane [24]. FePc produced CO but with low FE and decreasing activity for repetitive experiments. Theoretical analysis based on the Hückel model suggested CO desorption occurs for metal ions with a doubly occupied d_{z^2} orbital while further reduction is possible if CO is σ-bound to the metal [25]. The effect of CO_2 pressure was studied using GDEs impregnated with CoTPP or FeTPP [26]. The reduction wave of $Co^{II/I}TPP$ (> –1.0 V vs Ag/AgCl) was unobservable under Ar due to low concentration of adsorbed CoTPP, but the catalytic wave for H_2 production was observed. The effect of pressure on catalytic potential was evident in a *ca*. 100 mV positive shift for 20 atm CO_2 vs. 1 atm (Fig. 1~~Fig. 1~~). The CVs of CoTPP supported GDE show the unusual curvature toward the low-voltage especially under high CO_2 pressure, however, the authors did not give a clear explanation except that the waves were caused by electrocatalytic reduction around the potential where $Co^{II}TPP$ is reduced to $Co^{I}TPP$ (–0.8 V vs Ag/AgCl in DMSO or DMF). Faradaic efficiencies for CO were also increased at a 100 $mA.cm^{-2}$ current density. For CoTPP, the FE increased from 75 to 97% while for FeTPP an increase from 42 to 75% was observed (entry 9). Catalysis occurred near the $M^{II/I}$ potentials in DMF, and reactivity of the M(I) oxidation state was presumed.

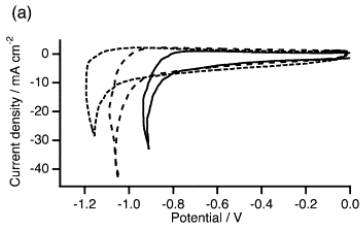

Fig. 1. Effect of CO_2 pressure on the cathodic CVs at a CoTPP supported GDE: under Ar (small dash), atmospheric CO_2 (large dash), and 20 atm CO_2 (solid line). The reference electrode was Ag/AgCl and scan rate was 50 mV.s^{-1}. Reprinted from ref. [26] with permission from Elsevier, Copyright 1999.

Gas diffusion electrodes with CoTMPP, CoPc, or Co(tBuPc) adsorbed on activated carbon fibers produce CO with 70% FE (entry 10) in a $KHCO_3$ aqueous solution under CO_2 [27]. The carbon fibers were loaded from organic solutions of the catalysts, and the adsorption limit for CoTPP was found to be 9 wt% of the catalyst on the carbon fiber surface which is 16% of the theoretical coverage. Loading was found to agree with the wetted area suggesting the catalysts are absorbed up to a certain depth upon which full pore width is occupied. Maximum current densities for CO production were achieved from −1.35 to −1.40 V vs. SCE. Current efficiencies for CO production with cobalt catalysts adsorbed on activated fibers, which have slit-shaped pores of ca. 2 nm width, showed an inverse dependence on catalyst dimensions and electrocatalytic performances as expected from the benefit of the so-called nanospace effect. However, Co(tBuPc) adsorbed on an activated carbon support, which has a much wider distribution in pore size dimension, was more effective with 85 % FE for CO production.

An interesting application of CO_2 electroreduction by CoPc-type catalysts is quantitative CO_2 analysis using the rotating ring-disk electrode and N,N′,N″,N‴-tetramethyltetra-3,4-pyridoporphyrazinoCo(II) (Co(tmtppa)) on a Nafion® protected carbon disk (entry 11) [28]. The film exhibited a $Co^{II/I}$ couple at +0.25 V vs. SCE and two pH dependent ligand based reductions near −0.25 and −0.7 V. At potentials more negative than –1.0 V, proton reduction began and obscured any surface redox processes. While CO_2 reduction was assumed to occur after formation of the doubly-reduced Co(I) Pc radical anion, the possible involvement of a $3e^-$ reduced species was considered. CO was detected at the Pt ring by its oxidation at 0.4 V with current proportional to scan rate, implicating surface oxidation of CO at Pt. A linear response was observed for CO_2 concentrations ranging from 0.1 to 32 mM using a disk potential of −1.08 V (Fig. 2~~Fig. 2~~).

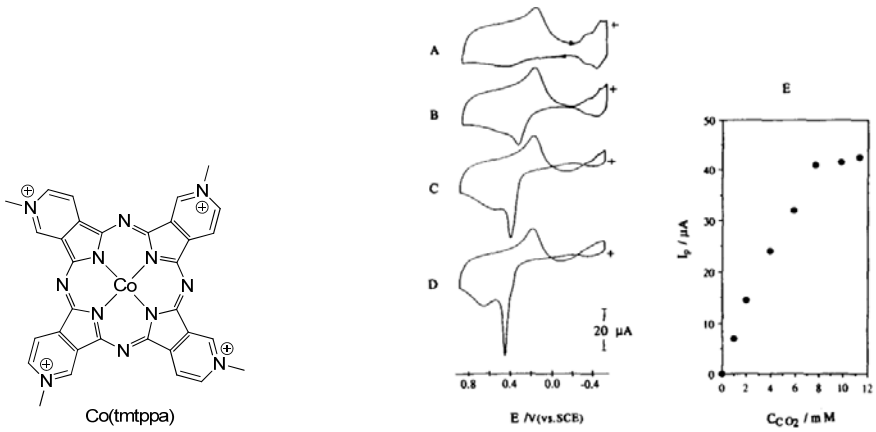

Fig. 2. Ring electrode cyclic voltammograms of a rotating ring (Pt)-disk (EPG/Co(tmtppa)/Nafion®) electrode recorded at a disk potential of −1.1 V in a solution at pH 5.5 containing various concentrations of CO_2: (A) 0.0 M; (B) 2.0×10^{-3} M; (C) 5.9×10^{-3} M; and (D) 1.13×10^{-2} M. Supporting electrolyte Britton-Robinson buffer, continuous scan, ring potential scan rate 100 mV.s^{-1},

rotation rate 900 rpm. (E) Ring CO oxidation peak currents near 0.4 V as a function of CO_2 concentration. Reprinted from ref. [28] with permission from Elsevier, Copyright 1996.

A microbial electrolysis cell (MEC) driven by current from a microbial fuel cell (MFC) [29] has been studied for CO_2 reduction (Fig. 3~~Fig. 3~~) [30]. In an MEC, oxidation of organic compounds provides protons and electrons for cathodic reactions. The active composite cathode was prepared by layer-by-layer dip coating of multiwalled carbon nanotubes (MWCNT) and FeTPP on indium tin oxide (ITO) or graphite. Scanning electron microscope (SEM) images showed an even surface distribution of the MWCNTs with nano-sized clusters of CoTAPc, and the presence of the catalyst was verified by absorption spectroscopy. The CV showed a CO_2 reduction peak at −0.5 V with current proportional to the number of adsorbed layers. The open circuit anode potential of the MEC was –0.3 V implying only 0.2 V external input was needed to drive CO_2 reduction. This input was generated by a single MFC with a cathode potential of 0.275 V and anode potential of −0.305 V across a 1000 Ω resistor. When connected to the MEC in series with a 10 Ω resistor, formic acid was produced with 74% FE. A maximum FE of 78% was achieved by controlling the anode potential to match the peak potential by CV (entry 12). The rate of formate production using the composite electrode was about 3 times that observed in the absence of MWCNTs and stable catalysis was measured for 10 consecutive 4 h batches. For more negative potentials, side reactions such as H_2 production competed with CO_2 reduction. While the authors claimed that this self-driven device is promising for CO_2 electrolysis since no external energy is needed, MFCs are producing a large amount of CO_2 together with electrons and protons from the oxidation of organic substrates (e.g., if sugar is used as a consumable substrate, then $C_{12}H_{22}O_{11} + 13H_2O \rightarrow 12CO_2 + 48H^+ + 48e^-$). Thus, while elegant in concept, practical application in CO_2 reduction chemistry will require a system which does not generate CO_2 as a byproduct.

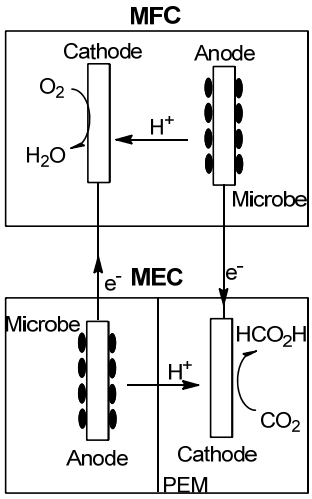

Fig. 3. Schematic representation of a microbial electrolysis cell (MEC) for CO_2 reduction using a MWCNT/CoTAPc cathode. The device is driven by electrons transferred from a microbial fuel cell (MFC). PEM = proton exchange membrane. Reprinted with permission from ref. [30], Copyright 2012 American Chemical Society.

In another example using MWCNTs as support on glassy carbon, adsorbed FeTPP showed higher activity and lower overpotential relative to drop coated FeTPPCl [31]. CO_2 was reduced to formic acid; however, the additives methyl viologen (MV^{2+}) as a redox mediator, formic dehydrogenase (FDH), and nicotinamide adenine dinucleotide (NADH) were required. The authors attributed efficient electrocatalysis of CO_2 by FeTPPCl adsorbed on MWCNT to (1) a decreased overpotential for reducing CO_2 to formic acid due to the interaction between MWCNTs and FeTPPCl, and (2) the excellent electrical conductivity of MWCNTs improved the electron transfer between CO_2 and the FeTPPCl active site to increase formic acid formation. However, the production of formate contrasts with the typical production of CO using FeTPPCl. Since this system requires MV^{+}, FDH and NADH, FeTPPCl may not be the active catalyst for formic acid production. It is known that FDH can catalyze not only oxidation of formate to CO_2, but also a hydride transfer from NADH to CO_2 to produce formate (not CO). Interestingly, reversible interconversion of CO_2 and formate by an electroactive FDH enzyme system with MV^{2+} and NADH has been achieved without any additional metal catalyst. [32]

As pointed out above, the identity of surface adsorbed active species is difficult to assess, especially at low catalyst loadings. While the onset of catalytic behavior (by CV) is often compared to solution data, it is possible that the adsorbed catalyst exhibits different potentials and/or substrate binding affinity. Indeed, the electronic structure of MTPP changes upon surface adsorption [33-40]. On Ag(111), X-ray photoelectron spectroscopy (XPS) showed charge transfer from FeTPP and CoTPP due to interaction with the surface (Fig. 4~~Fig. 4~~). A new valence state in the UV photoelectron and scanning tunneling spectra (UV and STS) showed covalent character between the MTPP and the surface. This coordinative character was reversed by axial coordination of NO corresponding to an increase in the metal oxidation state. DFT data supported the mutual interference of NO and Ag as axial ligands. The implication for catalysis of CO_2 reduction using adsorbed species is that electrode-catalyst surface interactions may increase electron density at the catalyst metal center in such a way that the transfer of a single electron may enhance substrate binding or even trigger catalysis at lower overpotentials compared to solution experiments.

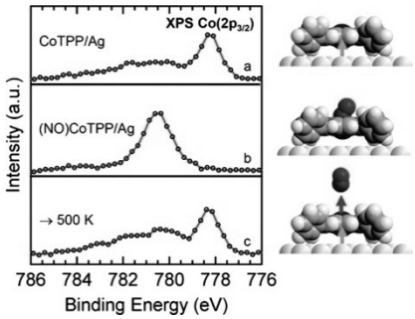

Fig. 4. Reversibility of the changes in the electronic structure induced by NO coordination: Co($2p_{3/2}$) XP spectra of CoTPP and (NO)CoTPP on Ag(111). (a) CoTPP monolayer, (b) (NO)CoTPP monolayer, (c) after heating the (NO)CoTPP monolayer to 500 K for thermal desorption of the NO ligand. Reprinted with permission from ref. [33], Copyright 2011 American Chemical Society.

Table 1 Location

B. Catalysts Covalently Grafted to Electrodes.

Amide Linkages. There are several disadvantages to simple non-covalent adsorption of catalysts onto electrode surfaces. Stability of the modified electrode is a forefront concern while the impact of adsorption on catalytic properties is difficult to predict. Structure-activity relationships are difficult to surmise since solution properties may not be conserved on a surface. The following discussion summarizes experiments using covalent linkage of the catalyst to the electrode. These methods allow more direct translation of solution properties to the surface, and often better control of catalyst loading, film thickness, and local pH environment. Relevant data are summarized in Table 2.

A CoTPP-pyridine complex immobilized on a glassy carbon electrode (Fig. 5A) exhibited high electrocatalytic activity and stability for CO_2 reduction [41]. The covalent linkage of pyridine to glassy carbon through amide bonds is achieved by oxidation of the carbon surface with H_2SO_4, treatment with $SOCl_2$ and then 4-amino-pyridine [41]. The presence of the amidine pyridine linker was confirmed by the C=O stretch at 1665 cm^{-1} and pyridine C=C and C=N stretches at 1610 and 1537 cm^{-1}. CoTPP was bound to the pyridine ligand in axial sites from benzene and its coordination to pyridine on the surface was confirmed by the matching of the Soret band at 440 nm in the diffuse reflectance spectrum to the visible spectrum of CoTPP in pyridine (Fig. 5~~Fig. 5~~A and B). In water, the modified electrode showed catalytic waves for H_2 and CO formation under He and CO_2, respectively, near the $Co^{II/I}$ couple in pyridine (Fig. 5C). Extended electrolysis at −1.2 V produced CO with >50% FE and 10^5 turnovers (Table 2, entry 1). Under optimized conditions (entry 2), CO was evolved with 92% FE, 300 mV overpotential, and over 10^7 turnovers [42]. The surface coverage, assuming a monolayer, was 10^{-12} mol.cm^{-2}. In solution, formate was produced with only 10% FE and rapid decomposition occurred thus validating the surface confinement as a method to stabilize the catalyst.

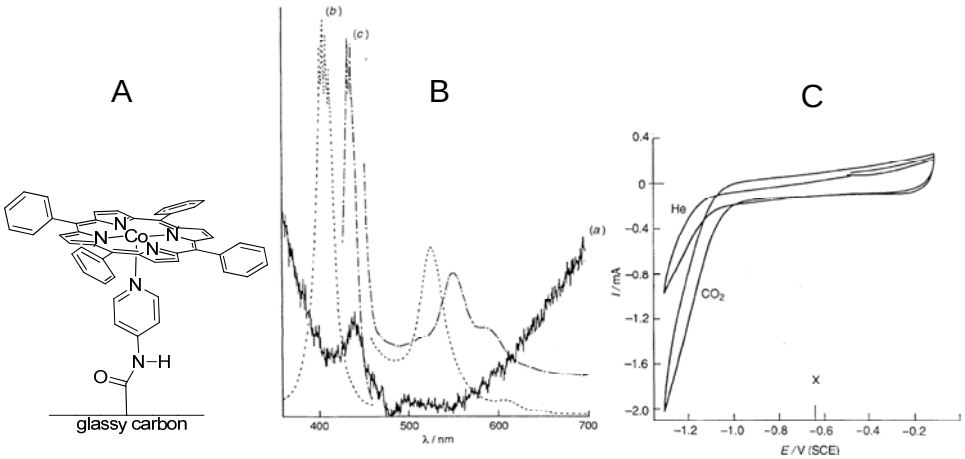

Fig. 5. (A) Schematic of CoTPP linked to glassy carbon through a 4-amide pyridine ligand. (B) Diffuse reflectance UV-vis spectrum of the CoTPP modified electrode (a), UV-vis spectrum of CoTPP (b) and CoTPP(pyridine) in CH_2Cl_2 (c). (C) CV of the CoTPP electrode in pH 6.86 phosphate buffer in the presence of CO_2 (a) or He (b) at room temperature. Scan rate 1 $mV.s^{-1}$. Reproduced from ref. [41] with permission from The Royal Society of Chemistry.

The same immobilization technique was extended to CoPc, CoNc, CoTMeOPP and hydrophobic vitamin B12 [43]. Catalytic activity for H_2 evolution was observed together with CO_2 reduction. An insightful observation regarding the mechanism was made using CV experiments: if the switching potential was negative of proton reduction current under N_2, the anodic return sweep exhibited a wave with potential varying from −0.35 to −0.78 V among these complexes. This feature was not observed if the switching potential was kept positive of the H_2 evolution potential and also disappeared for CVs under CO_2. These observations suggest that the anodic wave under N_2 is due to re-oxidation of a H_2-producing intermediate (i.e., a cobalt hydride), which is also consumed by the reaction of CO_2 (and thus not re-oxidized at the electrode).The oxidation peak was thus assigned as oxidation of a Co hydride that reacts with CO_2. The authors proposed that the produced Co–COOH species converts to Co(II), CO, and H_2O by further addition of H^+ and an electron. According to the CV data in DMSO, the complexes could be reduced by a second electron. Therefore, the loss of the anodic feature could be due to a preferential interaction of CO_2 with the doubly-reduced species to produce CO. Furthermore, a product of the reaction of M–H with CO_2 is normally considered to be M–OCHO (i.e., a precursor of $HCOO^-$), not M–COOH (a precursor of CO). During electrolysis under CO_2, the CoNc and CoPc (with the most positive potentials) exhibited the highest current densities (for mainly H_2 production) while CoTPP showed the highest current efficiency for CO (Table 2 entry 3).

Aminopyridine Radicals. A second approach to covalent linkage of a pyridine ligand to an electrode as a tether for Fe and Co catalysts is electrooxidation which triggers chemical bonding of the radical cation to glassy carbon. The method was investigated with 4-aminopyridine, 4-aminoethylpyridine, and imidazole. CoTPP was introduced from hot benzene/CH_2Cl_2 [44]. The amount of immobilized ligand was estimated as 9×10^{-11} $mol.cm^{-2}$. The reductive CV in pH 6.8 phosphate buffer exhibits the same anodic return wave discussed above for amide-linked pyridine electrodes (Fig. 6~~Fig. 6~~). Again, the feature is absent under CO_2 or for CoTPP adsorbed directly on glassy carbon. The good agreement found between the charge density of the anodic wave and the surface loading of CoTPP (1.6×10^{-8} $mol.cm^{-2}$) obtained by ultrasonic dissolution suggested a $1e^-$ oxidation process for the anodic return wave. Notably the ultrasonic dissolution measurements revealed the presence of 100-fold more CoTPP than available ligand sites suggesting that a monolayer of CoTPP was bound through pyridine coordination and additional catalyst was stacked upon the base layer of CoTPP. Heavy rinsing with CH_2Cl_2 removed the stacked molecules as shown by the absence of the anodic hump and increased the efficiency for CO production during electrolysis. Faradaic efficiencies of 39 − 59% were reported with the remaining current reducing H^+ (entry 5).

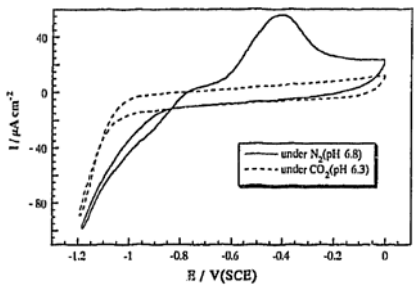

Fig. 6. Cyclic voltammograms at 50 mV.s^{-1} of CoTPP bonded to glassy carbon in N_2 and CO_2 atmospheres in pH 6.8 phosphate buffer. The bridging compound is 4-aminopyridine. Reprint from ref. [44] with permission from Elsevier, Copyright 1997.

The amino-pyridine methodology has been extended to Co(benzoPor) (benzoPor = tetrabenzoporphyrin) with no effort to remove the stacked molecules from the pyridine-bound surface layer [45,46]. Adsorbed Co(benzoPor) was inactive for electrochemical CO_2 reduction, but showed enhanced photoelectrochemical current. The authors viewed the Co(benzoPor) excited state as a source of reductive driving force and examined the CVs during illumination of the Soret band at 420 nm and Q bands at 525 and 625 nm. Irradiation of the electrode at 625 nm produced a significant positive shift in the CV under CO_2 (Fig. 7~~Fig. 7~~). The same shift was obtained using $[Ru(bpy)_3]^{2+}$ as a sensitizer in solution for 420 and 525 nm. Product analysis was not reported.

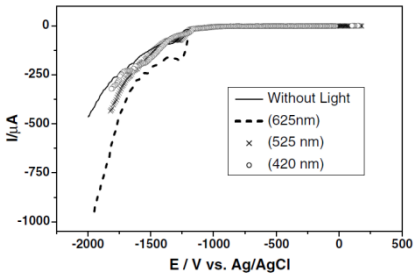

Fig. 7. Cyclic voltammograms at 5 mV.s^{-1} showing the response of the supramolecular electrode toward the reduction of CO_2 with and without illumination at different wavelengths. Reprint from ref. [46] with permission from Elsevier, Copyright 2009.

Polymerized Ligands. A third approach to electrode preparation involves formation of a film by electropolymerization of monomers such as 4-vinylpyridine or pyrrole and drop casting CoPc onto the film or casting a mixture of dissolved polymer and catalyst directly onto the electrode [47-49]. A CoPc/PVP (poly-4-vinylpyridine) film exhibited similar UV-vis properties to those observed in pyridine suggesting a surface Co-pyridine interaction. The sharp bands of CoPc/PVP compared to the broadened features of a CoPc solid layer imply homogeneous dispersion within the film. A reactive surface coverage of 5.0×10^{-12} mol.cm^{-2}, corresponding to a monolayer was determined. The $Co^{II/I}$ couple was found to exhibit $1H^+/1e^-$ pH dependence below pH 5.3 from −0.62 to −0.38 V vs. SCE attributed to protonation on the peripheral ring nitrogen. The ligand-based reduction in the film was observed at −0.7 V at pH 2.1 and showed a 75 mV/decade dependence on pH attributed to a second protonation. The CV of the CoPc/PVP electrode under CO_2 showed much larger catalytic current than CoPc adsorbed on graphite

under the same conditions and CoPc/PVP produced more CO with better selectivity. Since proton reduction was observed concurrent with CO_2 reduction, the dependence on pH and applied potential were investigated to improve selectivity. Initially, the best CO/H_2 selectivity (~3) was found at pH 6.8 with turnover numbers *ca*. 6×10^5. In this case, a mechanism involving reaction of $[Co^I(PcH^\bullet)]^-$ (i.e., the doubly-reduced species with the protonated Pc ligand) with CO_2 to form HOOC–CoPc via a proton transfer reaction from the protonated ligand was invoked. Later, the system was optimized with 1.2×10^{-10} mol.cm^{-2} at pH 5 and −1.2 V vs. Ag/AgCl providing $CO/H_2 = 6$ (entry 8) [48]. The pH-dependent behavior was attributed to partial protonation of pyridine residues surrounding the catalyst functioning as proton donors and acceptors, possibly functioning via a concerted proton transfer mechanism. A steady state concentration of $[Co^IPc]^-$ was found by electronic spectra measured during reduction under CO_2 confirming the reactivity of $[Co^I(Pc^{\bullet-})]^{2-}$ (or $[Co^I(PcH^\bullet)]^-$) since the later species did not accumulate during catalytic conditions in which it reacts rapidly with CO_2.

An electrode prepared by electropolymerization of pyrrole followed by drop casting a solution of CoPc from THF (CoPc/PPy, PPy = polypyrrole) exhibited an onset potential for CO_2 reduction 160 mV more positive than a PPy film without catalyst [49]. SEM imaging showed smooth surface coating of the PPy film and a crystalline porous structure with cast CoPc. The CV under CO_2 in $MeCN/H_2O$ exhibited catalysis at −0.18 V vs. Ag/AgCl, and extended electrolysis produced formic acid with ~72% Faradaic efficiency (entry 9) compared to 59% for the PPy electrode. CO_2 reduction at such mild potentials even without the catalyst is somewhat suspicious and points to a major role of the PPy film even without catalyst coating. Furthermore, production of formate in this system (vs CO and H_2) [47-49] illustrates that *a priori* prediction of product distribution for a given catalyst is not possible since electrode preparation and catalytic conditions are clearly important elements in the reduction of CO_2.

Functionalized Ligands. The fourth category for preparing functionalized electrodes involves direct electrode modification using specialized ligands designed with functional groups for polymerization or covalent reactions with electrode surfaces. In this regard, Co Ni, and Fe complexes with aminophthalocyanines (TAPc) were electropolymerized on glassy carbon [50]. CoTAPc produced formic acid while FeTAPc produced formaldehyde and H_2. No carbon products were detected using the polymerized free ligand. Poorly defined peaks were observed in the CV but the current discharge due to CO_2 reduction occurred cathodic of the doubly-reduced species, invoking injection of a third electron to trigger catalysis. Electrolysis of the CoTAPc polymer at −1.0 V yielded 7.9×10^4 turnovers of formate after 1.5 h. The FeTAPc polymer was not stable and small amounts of formaldehyde were detected. Electrochemical impedance spectroscopy revealed important morphological differences among polymers with varied metal ions.

Recently, a Co tetrakis(4-aminophenyl)porphyrin (TAPP) was electropolymerized on ITO and catalysis was examined in the room temperature ionic liquid 1-butyl-3-methylimidazolium tetrafluoroborate ($BMImBF_4$) [51]. The ionic liquid functions as solvent and electrolyte in this experiment. The film was prepared by 50 anodic cycles in DMF and any remaining NH_2 groups were electro-oxidized in water. SEM showed a heterogeneous distribution due to localized formation of oligomers. Stabilization in $BMImBF_4$ produced a more homogeneous surface due to intercalation of ions in the surface. The absorption spectrum of the film confirmed retention of the CoTAPP structure. Under N_2, a quasi-reversible $Co^{II/I}$ couple was observed at −0.75 V vs. Ag/AgCl. Under CO_2, a current

increase at the $Co^{II/I}$ couple prompted assignment of Co(I) as the active species; however, the $Co^{II/I}$ wave is visible in the catalytic current suggesting further reduction accelerates catalysis (Fig. 8~~Fig. 8~~). Electrolysis at −0.8 V produced CO with 65% FE (entry 12). After 4h, about 25% of the activity was lost (by CV). Impedance spectroscopy suggested CO_2 inclusion in the electric double layer decreases charge transfer resistance due to deformation and loss of density. The oxide acceptor for production of CO was not discussed. Presumably CO_2 is the oxide acceptor since protons should be scarce in the medium.

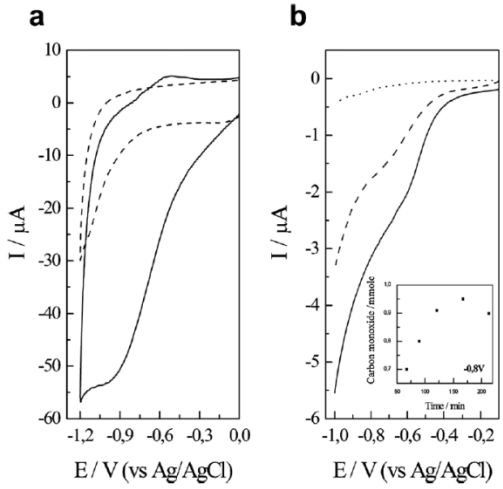

Fig. 8. (a) Cyclic voltammetry of the bare ITO electrode (dashed line) and the ITO/Poly-CoTAPP modified electrode (solid line) in $BMImBF_4$; scan rate 100 $mV.s^{-1}$. (b) Electrochemical behavior measured by linear sweep voltammetry at 5 $mV.s^{-1}$ of the bare ITO electrode (dots) and the Poly-CoTAPP modified electrode under N_2 (dashed line) and CO_2 (solid line) in $BMImBF_4$. Inset: CO production over time. Reproduced from ref. [51] with permission from The Royal Society of Chemistry.

Co porphryin has been attached to boron-doped diamond electrodes through triazolyl linkages (Fig. 9~~Fig. 9~~) [52]. Following functionalization of the diamond surface with alkyl azides, the 4-phenyl acetylene functionalized $CoTPP(CC)_8$ was attached via Cu-catalyzed cycloaddition. Its presence was verified by a decrease in azide IR signatures and observation of the Co(2p) region by X-ray photoelectron spectroscopy. The surface coverage was 3.8 × 10^{13} Co cm^{-2}. Electrocatalytic CO_2 reduction in acetonitrile was stable for >1000 cycles at −1.8 V with an estimated turnover frequency of 0.8 s^{-1}. The doubly reduced species was suggested as the active catalyst and CO was the only product detected.

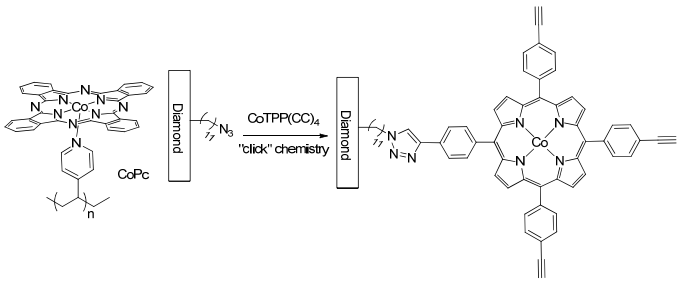

Fig. 9. Representation of covalent CoTPP modified boron-doped diamond electrodes [52].

Table 2 Location

III. HOMOGENEOUS CATALYSIS

A. Electrochemical CO_2 Reduction

The reduction of CO_2 by water soluble tetrasulfonated CoPc (CoTScPc) at an amalgamated Pt plate electrode was carried out as early as 1977 [53]. Catalytic current was observed around −1.3 V vs. SCE but the current depended on the initial potential and holding time, suggesting varied adsorption onto the electrode. Under similar conditions, CoTPPS reduced CO_2 to formate at −1.3 V while the Fe complex was not active [54].

A cofacial dinuclear metalloporphrin CoTPPS//Co-pTMPyP (Fig. 10~~Fig. 10~~) prepared by self-assembly of the cationic and anionic porphyrins is catalytically active in aqueous DMSO at −1.8 V vs. Ag/Ag^+ [55] The equilibrium constant for formation of the dinuclear structure was estimated as 10^6 M^{-1} in aqueous DMSO. The CV is essentially the sum of CVs for each individual complex and CO_2 reduction was attributed to Co(I) of Co-pTMPyP although the exact oxidation state at this stage was difficult to determine due to the presence of several ligand-based reductions. Based on the CVs, the CoTPPS functioned only as an "electron mediator", a term which the authors previously used to describe it as a redox-active electron donor to accelerate electron transfer to the catalytic metal. [56] In this case the metal ion identity of the mediator component was not essential, and similar catalytic results were achieved with CuTPPs.

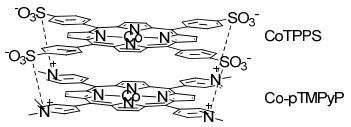

Fig. 10. Cofacial dinuclear porphryin complex prepared by self-assembly [55].

Co porphryins with phenylazomethine dendrimers catalyze CO_2 reduction in DMF assisted by lanthanide ions as strong Lewis acids [57]. Under N_2, the CV showed characteristic $Co^{II/I}$ waves near −1.3 V vs. $Fc^{+/0}$, and a catalytic current was triggered at this wave under CO_2. Comparison among different generations revealed a maximum efficiency for the third generation dendrimer and a decrease in activity of the fourth generation structure attributed to steric effects. A non-symmetric third generation dendrimer showed the greatest current attributed to accessibility of the Co center to CO_2 while maintaining the function of the dendrimer such as binding sites for Ln^{3+}. No product analysis was reported.

Iron tetraphenylporphryins have received considerable attention as homogeneous electrocatalysts for reduction of CO_2 to CO in DMF due in part to product selectivity, stability, and impressive rates. Early experiments revealed catalysis and the product CO as indicated by the $Fe^{II/I}$(CO) wave on the return scan [58] while advancement in the

system understanding is revealed by recent experiments showcasing the concerted nature of electron transfer, proton transfer, and C−O bond cleavage [59]. The FeTPP exhibits clear $Fe^{III/II}$, $Fe^{II/I}$, and $Fe^{I/0}$ couples (Fig. 11~~Fig. 11~~), the last of which (at −1.64 V vs. SCE) develops a catalytic current under CO_2. The active catalyst is best described using the Fe(0)TPP resonance structure in agreement with experimental reactivity and Raman spectroscopy [60-62]. In dry solvent, CO_2 is proposed as the oxide acceptor thereby generating CO_3^{2-} and few catalytic turnovers are achieved due to destruction of the TPP ligand by carboxylation. The rate of catalysis and durability were enhanced by the addition of Mg^{2+}, Na^+, Li^+, Ba^{2+}, or Al^{3+} ions, although Mg^{2+} was the most effective [63]. Two mechanisms were proposed to explain the temperature-dependent cyclic voltammograms. At −40 ºC the carbene type complex, $[Fe^{II}(TPP)(CO_2^{2-})]^{2-}$, formed via the reaction of Fe(0) with CO_2 reacts first with another carbon dioxide molecule. Decomposition of this species into Fe^{II}(TPP)CO and carbonate is accelerated by a Lewis acid. At room temperature, Mg^{2+} reacts directly with $[Fe^{II}(TPP)(CO_2^{2-})]^{2-}$. For monovalent Lewis acids, the catalysis is second order in $[CO_2]$ and $[M^+]$, suggesting a mechanism in which $[Fe^{II}(TPP)(CO_2^{2-})]^{2-}$ reacts with CO_2 and the intermediate is stabilized in two separate steps by Li^+. This species decomposes to Fe^{II}(TPP)CO and Li_2CO_3 [64]. Deviation of the catalytic wave from S-shape was explained by precipitation of carbonates on the electrode.

A major breakthrough in FeTPP catalysis was realized by the addition of weak Brönsted acids such as CF_3CH_2OH [65]. In DMF containing 0.1 M Et_4NClO_4 at a hanging mercury drop electrode, the ratio of catalytic current (i_c) to the $Fe^{I/0}$ current in the absence of CO_2 (i_p) was only 1.8 but reached 131 with 1.47 M CF_3CH_2OH. The FE for CO production was 94% whereas it was only 70% with Lewis acid additives. In preparative scale experiments, current is limited by cell geometry, not the rate of catalysis. About 75% of the catalyst remained intact after passage of 225 C during bulk electrolysis. The scope of acid synergy was expanded to 2-pyrrolidone, 1-propanol, and mixtures of water in 1-propanol (Fig. 12~~Fig. 12~~) [66]. It was found that selectivity for CO and stability both increased as the acid becomes more acidic although FeTPP will catalyze proton reduction if stronger acids ($pK_a < \sim 9$) are added. Kinetic analysis revealed first-order dependence on $[CO_2]$ and second-order dependence on $[CF_3CH_2OH]$, at least in the low concentration region where the voltammetric response exhibits the S-shape characteristic of large substrate excess which remains unchanged from the bulk concentration (Fig. 13~~Fig. 13~~). At higher concentrations, the appearance of a peak-shaped wave was attributed to self-inhibition by the CO product through adsorption on the Hg thus inactivating portions of the electrode. In agreement with theory is the scan-rate dependence in which the peak shape becomes less pronounced at higher sweep rates. Notably, the turnover number in preparative scale electrolysis is significantly less than that calculated from voltammetry, suggesting the interference of ohmic drop in bulk experiments.

The catalytic response of FeTPP in the presence of water, phenol, trifluoroethanol, and acetic acid was further analyzed to reveal an intimate detail of the catalytic mechanism, namely, the concerted C–O cleavage with electron and proton transfer as the rate determining step [67]. There is a pK_a dependence on the rate determining step and stepwise proton / electron transfer was ruled out assuming protonation of a CO_2 radical anion should be near the diffusion limit regardless of pK_a.

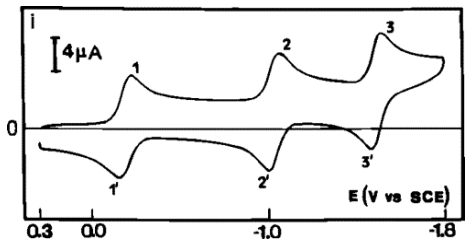

Fig. 11. Cyclic voltammetry of FeTPP (1 mM) in DMF at a glassy carbon electrode. Scan rate = 100 mV.s^{-1}. Reprinted with permission from ref. [66], Copyright 1996 American Chemical Society.

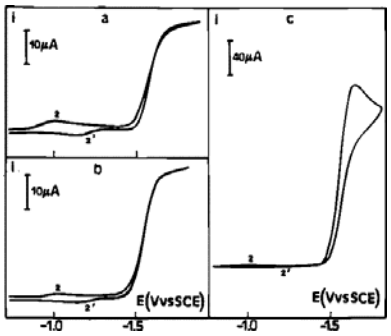

Fig. 12. Cyclic voltammetry of FeTPP (0.5 mM) in DMF under 1 atm CO_2 in the presence of 0.51 M 2-pyrrolidone (a), 6.66 M 1-propanol (b), and 1.47 M CF_3CH_2OH (c) at Hg, scan rate 100 mV.s^{-1}. Reprinted with permission from ref. [66], Copyright 1996 American Chemical Society.

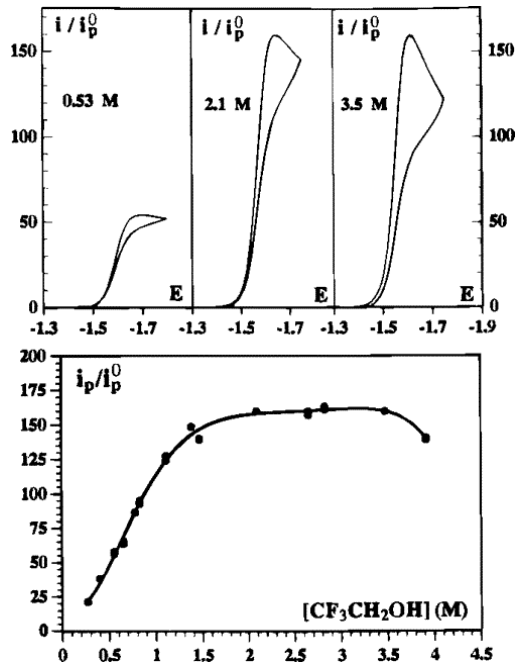

Fig. 13. Cyclic voltammetry of the reduction of CO_2 (1 atm) in DMF catalyzed by 1 mM FeTPP with varied concentrations of CF_3CH_2OH. Scan rate 100 mV.s^{-1}. Reprinted with permission from ref. [66], Copyright 1996 American Chemical Society.

Further remarkable advancement of FeTPP electrocatalysis in DMF was achieved by introduction of phenol groups in ortho positions of the TPP phenyl groups (TDHPP) to speed up CO_2 reduction by providing a pre-positioned proton source for the $2e^-/2H^+$ conversion of CO_2 to CO [68]. Comparison of the catalytic rate constant ($k_{cat} = 2k[CO_2]$) of 1.6×10^6 s^{-1} for FeTDHPP with that for FeTPP with external 3 M phenol (3.2×10^4 s^{-1}) suggested the proximal proton source in FeTDHPP is equivalent to 150 M phenol. The authors describe that the exact mechanism of the phenol influence in CO_2 reduction is not known, however, it is likely to be a push-pull type interaction between a proton and an electron as previously proposed for other acids [66]. Electrolysis at −1.16 V (well below the $Fe^{I/0}$ couple at −1.33 V) produced CO with 90% FE and 0.31 mA.cm^{-2} with 50 million turnovers over 4 hours of electrolysis. Comparison to the methylated catalyst FeTDMPP, which was less active, further supported the involvement of internal protons in the catalysis.

A related catalyst with prepositioned phenol groups and perfluorination of the remaining phenyl groups ($FeTDHPPF_{10}$) is more active than FeTDHPP while its $Fe^{I/0}$ couple is less negative [59]. In this case, the catalytic response is preceded by a one-electron wave indicating that the "Fe(0)–CO_2" adduct is stabilized by phenolic hydrogen bonding that is also confirmed with DFT calculations. However, injection of a third electron is required to commence catalysis. The rate constants for CO_2 adduct formation were estimated as $> 5 \times 10^6$ M^{-1}.s^{-1} and 3×10^5 M^{-1}.s^{-1} for FeTDHPP and $FeTDHPPF_{10}$, respectively, from the scan-rate dependent behavior of the pre-wave. Since the adduct is protonated by internal phenolic groups, the potential for the second electron transfer is only slightly cathodic of the $Fe^{I/0}$ couple. It was suggested that concerted re-protonation of internal OH groups by phenol with electron transfer, proton transfer, and C–O bond cleavage is also possible. The remarkable roles of the prepositioned

phenol groups resemble the 2nd coordination-sphere effect previously found for interconversion of H^+/H_2 and $CO_2/HCOO^-$ using other molecular metal catalysts[69-71].

B. Photochemical CO_2 Reduction

Photochemical experiments are useful probes for studying Fe and Co porphyrins, phthalocyanines, corroles, and corrins and their reactions with CO_2 since the absorption spectra of each oxidation state exhibit distinct features which are readily monitored. Additionally, pulse radiolysis with a short electron pulse is used to determine reaction kinetics by monitoring differential absorption spectra. Photocatalytic CO_2 reduction is possible if the photo-produced species reacts with CO_2, releases product, and re-enters the catalytic cycle. Pertinent photochemical systems for CO_2 reduction are summarized in Table 3 and relevant equations are collected in Table 4.

First, iron porphyrins are considered [72]. Photolysis of $ClFe^{III}TPP$ with 325 nm < λ < 385 nm in DMF containing 5% triethylamine (Et_3N) as an electron donor yielded $Fe^{II}TPP$ through electron transfer with a quantum efficiency of *ca*. 0.05 (Scheme 1).

Scheme 1. Photochemical reduction of $Fe^{III}TPP$.

$$(Et_3N)(Cl)Fe^{III}TPP + h\nu \rightarrow Et_3N^{\bullet+} + Cl^- + Fe^{II}TPP$$

$$Et_3N^{\bullet+} + Et_3N \rightarrow Et_3NH^+ + Et_2NC^{\bullet}HCH_3$$

$$Et_2NC^{\bullet}HCH_3 + (Cl)Fe^{III}TPP \rightarrow Et_2N^+{=}CHCH_3 + Fe^{II}TPP + Cl^-$$

$$Et_3NFe^{II}TPP + h\nu \rightarrow Et_3N^{\bullet+} + [Fe^{I}TPP]^-$$

Continued photolysis generated $[Fe^{I}TPP]^-$ with low efficiency suggesting weaker interaction with Et_3N. The reaction was not quantitative and peaks due to hydrogenation products were observed. Under CO_2, the reduced $[Fe^{I}TPP]^-$ was converted to the Fe(II)–CO complex, which releases CO upon photolysis [73]. Throughout extended photolysis (> 150 hrs) CO was quantified by gas chromatography and the overall turnover number reached ~70 [72]. During photolysis, the chlorin was observed as a green solution which remained catalytically active. CO production ceased when the solution turned yellow indicating destruction of the ligand. Decomposition was slowed at lower concentrations since its primary path is presumed to be the reaction of $[Fe^{0}TPP]^{2-}$ with other porphyrin species.

Scheme 2. Radiolytic reduction of water-soluble Fe porphryins showing the formal Fe-oxidation states, but ignoring the total charges due to complication of the peripheral charges.

$$H_2O \rightsquigarrow e_{aq}^-, H^\bullet, {}^\bullet OH, H^+, H_2, H_2O_2$$

$$H^\bullet/{}^\bullet OH + HCO_2^- \rightarrow H_2/H_2O + CO_2^{\bullet-}$$

$$(Cl)Fe(III)Por + e_{aq}^- \rightarrow Cl^- + Fe(II)Por$$

$$(Cl)Fe(III)Por + CO_2^{\bullet-} \rightarrow Cl^- + Fe(II)Por + CO_2$$

$$Fe(II)Por + CO_2^{\bullet-} \rightarrow Fe(I)Por + CO_2$$

Radiolytic reduction of various water soluble Fe porphyrins (FePor) also produced the Fe(I) complexes (Scheme 2) with small amounts of the phlorin anion and chlorin. In alkaline solution, the Fe(I) porphyrins are stable for many hours but decay more rapidly at lower pH. Pulse radiolysis of Fe(II) porphyrins was used to analyze short-lived species in aqueous solution. Bleaching of the Soret band along with formation of absorptions below 520 nm and 600 – 840 nm indicated formation of Fe(I)Por as the first product. Interestingly, the Fe(I) complex of oTMPyP (see Chart 1) exhibits complicated decay behavior attributed to varied reactivity among the four atropisomers of the ligand. The decay obeyed a second-order rate law with $k = (1.5 \pm 0.5) \times 10^8\ M^{-1}.s^{-1}$ for the first step. Results are explained by a disproportionation reaction of Fe(I)Por to produce Fe(II)Por and Fe(0)Por. The Fe(0)Por reacts with water, protons, or CO_2 to produce intermediates which are protonated to yield H_2 or CO, and the Fe(0) state is implicated as the reactive species in photolysis experiments.

Photochemical and radiolytic studies of Co porphyrins were undertaken to characterize reduced species and examine their reactions with CO_2 [74]. In aqueous solution, radiolytic reductions of Co(III) to Co(II) and then to Co(I) were quantitative reactions yielding a stable Co(I) product at high pH. Pulse radiolysis of the Co(I) solution showed bleaching of the Co(I) absorption at 550 nm and broad absorptions from 640 – 800 nm, different from spectra of π-radical anions of Zn, Al and Sn [75-77] suggesting the product is Co(0) formed by reaction of Co(I) with e_{aq}^- (Table 4, eq. 7). A slower reaction of Co(I)-mTMPyP with $CO_2^{\bullet-}$ ($k \sim 5 \times 10^9\ M^{-1}.s^{-1}$) yielded a spectrum with features different from the Co(0) species suggestive of adduct formation followed by decomposition to CO and Co(II). Cyclic voltammetry in butyronitrile showed catalytic current under CO_2 upon reduction to Co(0) [74,78]. The reaction is first order in [catalyst] and [CO_2]. Since the Co(0) species are short-lived in water, sodium reduction was undertaken under static vacuum using dry THF. Smooth reduction to Co(I) and Co(0) was observed. While Co(I) did not react with CO_2, the Co(0) solution quickly produced the spectrum of Co(I) upon introduction of CO_2 and gradually changed to the spectrum of Co(II). Since the reaction of CO_2 with Co(0) should release CO and Co(II), the persistence of a Co(I) spectrum is attributed to comproportionation of Co(II) with Co(0). Photochemical reduction with Et_3N produced Co(II) and Co(I) while continued photolysis under CO_2 yielded CO with >300 turnovers.

Inefficient reduction to the reactive species of $[Co^0TPP]^{2-}$ or $[Fe^0TPP]^{2-}$ using Et_3N is a major limitation of photochemical reduction with the Co and Fe porphyrins discussed above. Two drawbacks are weak interactions of Et_3N with the Co or Fe centers and highly negative $M^{I/0}$ reduction potentials. Photochemical reduction efficiency was improved using *p*-terphenyl (TP) as a sensitizer [79]. The TP excited state is quenched by Et_3N to produce the $TP^{\bullet-}$ radical anion with a −2.45 V vs. SCE reduction potential which is sufficiently negative to produce Fe(0) and Co(0) [80]. Production of CO during photolysis was six times greater and ten times faster than in the absence of TP (Fig. 14~~Fig. 14~~) indicating efficient reactions of Co(II) and Co(I) with $TP^{\bullet-}$. These reactions (Table 4, eqs 11 and 12) were nearly diffusion controlled as measured by pulse radiolysis. Control experiments in the absence of porphyrin produced formate from the reaction of $TP^{\bullet-}$ with CO_2; however the rate of formate production at early times was low with porphyrin and reached the same concentration at later times. Accumulation of CO was found to limit catalysis and experiments with larger headspace produced more CO and for longer times. Catalysis resumed if CO was purged from the system and slowed if CO was initially introduced. $Fe^{III}T3CF_3PPCl$ was reduced by Na under static vacuum in THF to the Fe(0) state. CO does not bind to Fe(0) but binds to Fe(II) and Fe(I) in a reversible equilibrium. The spectrum of $Fe^{II}CO$ was also obtained by the reaction of CO_2 with Fe(0). No reactions of CO with Co(II), Co(I), or Co(0) were observed.

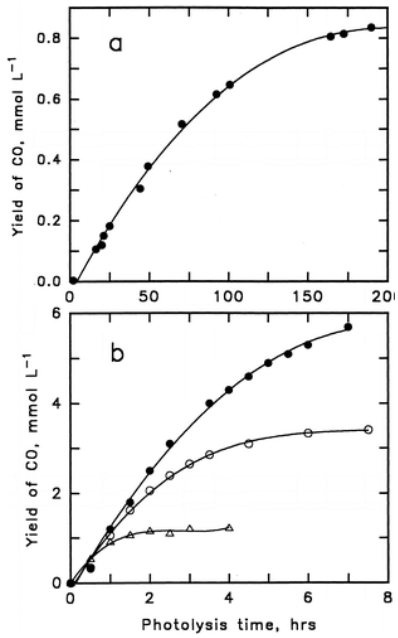

Fig. 14. Photochemical production of CO in CO_2-saturated acetonitrile containing 5% Et_3N: (a) 1 × 10−5 M $Co^{II}TPP$ with no TP; (b) with 3×10^{-3} M TP and various concentrations of $Co^{II}T3FPP$: 9 x 10^{-5} M (solid circles), 2.4 × 10^{-5} M (open circles), and 7 x 10^{-6} M (open triangles). The yield of CO refers to the total amount per unit volume of solution. Reprinted with permission from ref. [79], Copyright 1999 American Chemical Society.

Since hydrogenation of porphyrin rings during photochemical experiments is a degradation pathway, Co corrins (B_{12}) (Chart 2) with fewer double bonds, were examined as photocatalysts for CO_2 reduction using TP as a sensitizer and Et_3N as the sacrificial reductant [81]. Similar to Co porphyrins, reduction to the Co(0) state was necessary and CO, formate, and H_2 were produced at higher rates than CoTPP in parallel experiments. Pulse radiolysis of Co(I) showed rapid decay of e_{aq}^- and a slower reaction of $CO_2^{\bullet-}$ with Co(I) to form an adduct. Transient Co(0) reacts with water to form the hydride but decay of this species could not be observed separately.

Chart 2. Co corrins studied for photoreduction of CO_2.

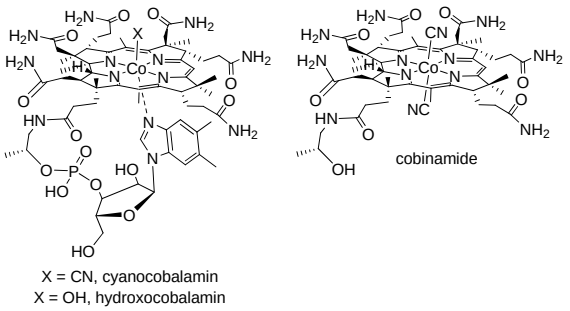

Photochemical and radiolytic techniques were also used to characterize the reduced species of Fe and Co phthalocyanines together with their tetra(*tert*-butyl)- and tetrasulfonated derivatives (Chart 1), and to determine reactivity toward CO_2 [82]. Radiolytic reduction of the Co(II) complex with TSPc produced the corresponding Co(I) (mixture of monomers and dimers) in quantitative yield. Likewise, the Fe(I) complex with TSPc was obtained in high yield and both compounds were stable for hours. The Co(I) complex was further reduced by $CO_2^{\bullet-}$ to form the CO_2 adduct. To clarify the intermediates of CO_2 reduction, stepwise reduction of Co^{II}TBPc was carried out using sodium mirror in THF. The doubly-reduced species, $[Co^{I}(TBPc^{\bullet-})]^{2-}$, reacted rapidly with CO_2 to form a complex, which decomposes to Co^{II}TBPc and CO. The decomposition seems to be enhanced by CO_2 acting as an oxide acceptor. Photoreduction in CH_3CN with Et_3N and TP produced Co(I) and Fe(I) but further reduction led to bleaching. Photochemical production of CO and formate was not as effective as with phthalocyanines due to hydrogenation of the ligand.

To complete the series of photochemical CO_2 reduction experiments, Fe and Co corroles were investigated (Chart 3) [83]. Lacking one meso bridge and bearing three anionic nitrogen ligands, corroles stabilize higher metal oxidation states. Thus it was proposed that the M(I) state could react with CO_2. Indeed, CV data confirmed the reaction of CO_2 at slightly more negative potentials than the $Co^{II/I}$ wave with Ph_3PCo(tpfc) (Fig. 15~~Fig. 15~~) or at the $Fe^{II/I}$ potential with $ClFe^{IV}$(tdcc) showing catalytic current. Spectroscopic characterization showed the reaction of CO_2 with the Fe(I) state to produce Fe(II) and CO together with a small amount of Fe^{II}CO. The Fe(II) species are produced by comproportionation of Fe(III) and Fe(I). Extended photoreduction of the M(II) state with Et_3N and TP produced peaks different from sodium reduction which first decreased and then were completely lost. Under CO_2,

H_2 and CO are evolved showing that the reaction of M(I) with H^+ competes with CO_2. Total turnovers were about 300.

Chart 3. Fe and Co corroles studied for photochemical CO_2 reduction.

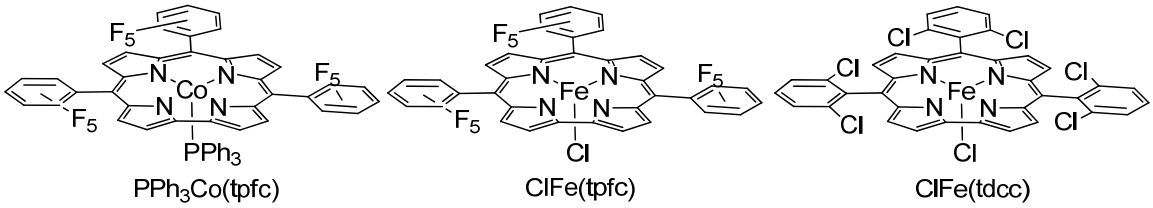

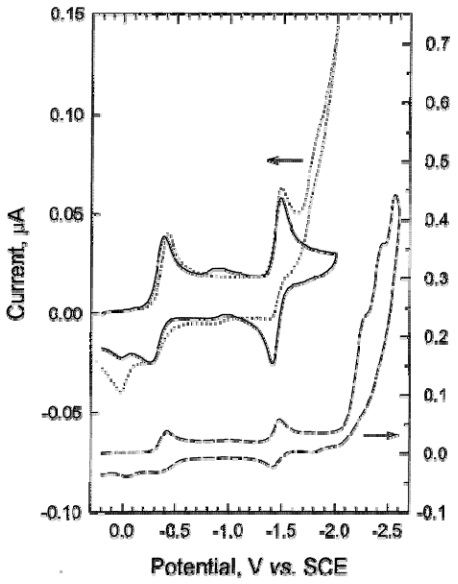

Fig. 15. Cyclic voltammograms of PPh_3Co^{III}(tpfc) in CH_3CN solution saturated with Ar (solid line) and CO_2 (dotted line). A wider scan of the Ar-saturated solution is shown by the dashed line. Scan rate 100 $mV.s^{-1}$. Reprinted with permission from ref. [83]. Copyright 2002 American Chemical Society.

Table 3 Location

Table 4 Location

IV. CONCLUSIONS AND OUTLOOK

In this review, we summarized electrochemical and photochemical CO_2 reduction with a variety of iron and cobalt complexes incorporating porphyrins and phthalocyanines. While CO_2 can bind to one-electron-reduced cobalt(I) complexes with partially saturated tetraaza-macrocycles such as a cobalt(I) complex with 5,7,7,12,14,14-hexamethyl-1,4,8,11-tetraazacyclotetradeca-4,11-diene [84], those of metalloporphyrins and metallo phthalocyanines cannot because the electron densities on these species are partially distributed on the conjugated ligands. Although there are some conflicting reports of CO_2 activation by one-electron-reduced Co(I) and Fe(I) porphyrins/phthalocyanines (without the ligand anion radicals), the active catalysts with metalloporphyrins are further reduced species as identified by cyclic voltammetry to have the metal in the formal oxidation state of zero. In the case of phthalocyanine complexes, the metal oxidation state is +1 with the ligand anion radical. Fe and Co corroles are lacking one meso bridge and bearing three anionic nitrogen ligands, therefore, metal(I) corrole complexes can react with CO_2. In each case, the species which react with CO_2 in solution have been identified in recent years using radiolytic or chemical reduction techniques.

Metalloporphyrins and metallophthalocyanines are visible light absorbers with extremely large extinction coefficients. However, yields of photochemically-generated active catalysts for CO_2 reduction are low due to the requirement of a photoinduced 2nd electron. This situation can be ignored in the case of electrochemical CO_2 reduction. Recent progress on efficient and stable electrochemical systems using FeTPP catalyst prepositioning of proton-donating phenol groups in the 2nd coordination sphere to carry out coupled proton-electron transfer within the catalytic cycle is remarkable. The incorporation of Lewis or Brönsted acids in the catalysts seems an outstanding direction not only to reduce overpotential but also to speed up the reaction.

Selectivity of the products (i.e., CO, $HCOO^-$, H_2, etc.) and long-term durability of cobalt and iron catalysts can be problematic especially when water is used as a solvent. Reduced Fe and Co porphyrins react with protons to produce metal hydride species, which are considered as intermediates for H_2 and $HCOO^-$ production, and in some cases even for CO production. Also, hydrogenation of the ligand due to the electron rich nature of the reduced catalysts may decrease the catalytic activity for CO_2 reduction. Advances in experimental techniques have revealed a wealth of mechanistic information in recent years, yet detailed thermodynamic and kinetic studies of proton and CO_2 binding to the reduced metal catalysts would help to understand the mechanisms for CO_2 reduction.

Ground-breaking research has to be continued to produce renewable fuels (CO, and ultimately further reduced species such as methanol and methane) via low-energy pathways using durable and selective earth-abundant catalysts for creating carbon-neutral energy sources.

Acknowledgements

We thank Drs. James T. Muckerman and David C. Grills for careful reading of this manuscript. The work at Brookhaven National Laboratory was carried out under contract DE-AC02-98CH10886 with the U.S. Department of Energy, Office of Science, Office of Basic Energy Sciences.

References

1. D'Alessandro DM, Smit B and Long JR. *Angew. Chem. Ind. Ed.* 2010; **49**: 6058-6082.
2. Schwarz HA and Dodson RW. *J. Phys. Chem.* 1989; **93**: 409-414.
3. Benson EE, Kubiak CP, Sathrum AJ and Smieja JM. *Chem. Soc. Rev.* 2009; **38**: 89-99.

4. Morris AJ, Meyer GJ and Fujita E. *Acc. Chem. Res.* 2009; **42**: 1983-1994.
5. Windle CD and Perutz RN. *Coord. Chem. Rev*. 2012; **256**: 2562-2570.
6. Qiao JL, Liu YY, Hong F and Zhang JJ. *Chem. Soc. Rev.* 2014; **43**: 631-675.
7. Lim RJ, Xie MS, Sk MA, Lee JM, Fisher A, Wang X and Lim KH. *Catal. Today*. 2014; **233**: 169-180.
8. Izumi Y. *Coord. Chem. Rev*. 2013; **257**: 171-186.
9. Costentin C, Robert M and Saveant J-M. *Chem. Soc. Rev.* 2013; **42**: 2423-2436.
10. Appel AM, Bercaw JE, Bocarsly AB, Dobbek H, DuBois DL, Dupuis M, Ferry JG, Fujita E, Hille R, Kenis PJA, Kerfeld CA, Morris RH, Peden CHF, Portis AR, Ragsdale SW, Rauchfuss TB, Reek JNH, Seefeldt LC, Thauer RK and Waldrop GL. *Chem. Rev.* 2013; **113**: 6621-6658.
11. Sakakura T, Choi JC and Yasuda H. *Chem. Rev.* 2007; **107**: 2365-2387.
12. Aresta M and Dibenedetto A. *Dalton Trans.* 2007: 2975-2992.
13. Truxillo LA and Davis DG. *Anal. Chem.* 1975; **47**: 2260-2267.
14. Araullomcadams C and Kadish KM. *Inorg. Chem.* 1990; **29**: 2749-2757.
15. Meshitsu.S, Ichikawa M and Tamaru K. *J. Chem. Soc. Chem., Commun.* 1974: 158-159.
16. Kapusta S and Hackerman N. *J. Electrochem. Soc.* 1984; **131**: 1511-1514.
17. Lieber CM and Lewis NS. *J. Am. Chem. Soc.* 1984; **106**: 5033-5034.
18. Christensen PA, Hamnett A and Muir AVG. *J. Electroanal. Chem.* 1988; **241**: 361-371.
19. Tanabe H and Ohno K. *Electrochim. Actta.* 1987; **32**: 1121-1124.
20. Abe T, Taguchi F, Yoshida T, Tokita S, Schnurpfeil G, Wohrle D and Kaneko M. *J. Mol. Catal. A: Chem.* 1996; **112**: 55-61.
21. Abe T, Imaya H, Yoshida T, Tokita S, Schlettwein D, Woehrle D and Kaneko M. *J. Porphyrins and Phthalocyanines*. 1997; **1**: 315-321.
22. Motoo S, Watanabe M and Furuya N. *J. Electroanal. Chem.* 1984; **160**: 351-357.
23. Mahmood MN, Masheder D and Harty CJ. *J. Appl. Electrochem.* 1987; **17**: 1223-1227.
24. Furuya N and Matsui K. *J. Electroanal. Chem.* 1989; **271**: 181-191.
25. Furuya N and Koide S. *Electrochim. Actta.* 1991; **36**: 1309-1313.
26. Sonoyama N, Kirii M and Sakata T. *Electrochem. Commun.* 1999; **1**: 213-216.
27. Magdesieva TV, Yamamoto T, Tryk DA and Fujishima A. *J. Electrochem. Soc.* 2002; **149**: D89-D95.
28. Zhang JJ, Pietro WJ and Lever ABP. *J. Electroanal. Chem.* 1996; **403**: 93-100.
29. Logan BE, Hamelers B, Rozendal RA, Schrorder U, Keller J, Freguia S, Aelterman P, Verstraete W and Rabaey K. *Environ. Sci. Technol.* 2006; **40**: 5181-5192.
30. Zhao HZ, Zhang Y, Zhao B, Chang YY and Li ZS. *Environ. Sci. Technol.* 2012; **46**: 5198-5204.
31. Zhao HZ, Chang YY and Liu C. *J. Solid State Electrochem.* 2013; **17**: 1657-1664.
32. Reda T, Plugge CM, Abram NJ and Hirst J. *Proc. Natl. Acad. Sci. U.S.A.* 2008; **105**: 10654-10658.
33. Hieringer W, Flechtner K, Kretschmann A, Seufert K, Auwarter W, Barth JV, Gorling A, Steinruck HP and Gottfried JM. *J. Am. Chem. Soc.* 2011; **133**: 6206-6222.
34. Seufert K, Auwarter W and Barth JV. *J. Am. Chem. Soc.* 2010; **132**: 18141-18146.
35. Auwarter W, Seufert K, Klappenberger F, Reichert J, Weber-Bargioni A, Verdini A, Cvetko D, Dell'Angela M, Floreano L, Cossaro A, Bavdek G, Morgante A, Seitsonen AP and Barth JV. *Phys. Rev. B*. 2010; **81**.
36. Gottfried JM and Marbach H. *Z. Phys. Chemie-Int. J. Res. Phys. Chem. Chem. Phys.* 2009; **223**: 53-74.
37. Buchner F, Warnick KG, Wolfle T, Gorling A, Steinruck HP, Hieringer W and Marbach H. *J. Phys. Chem. C*. 2009; **113**: 16450-16457.
38. Bai Y, Buchner F, Kellner I, Schmid M, Vollnhals F, Steinruck HP, Marbach H and Gottfried JM. *New J. Phys.* 2009; **11**.
39. Lukasczyk T, Flechtner K, Merte LR, Jux N, Maier F, Gottfried JM and Steinruck HP. *J. Phys. Chem. C*. 2007; **111**: 3090-3098.
40. Flechtner K, Kretschmann A, Steinruck HP and Gottfried JM. *J. Am. Chem. Soc.* 2007; **129**: 12110-+.
41. Atoguchi T, Aramata A, Kazusaka A and Enyo M. *J. Chem. Soc. Chem., Commun.* 1991: 156-157.
42. Atoguchi T, Aramata A, Kazusaka A and Enyo M. *J. Electroanal. Chem.* 1991; **318**: 309-320.
43. Aga H, Aramata A and Hisaeda Y. *J. Electroanal. Chem.* 1997; **437**: 111-118.
44. Tanaka H and Aramata A. *J. Electroanal. Chem.* 1997; **437**: 29-35.
45. Ramirez G, Lucero M, Riquelme A, Villagran M, Costamagna J, Trollund E and Aguirre MJ. *J. Coord. Chem.* 2004; **57**: 249-255.
46. Ramirez G, Ferraudi G, Chen YY, Trollund E and Villagra D. *Inorg. Chim. Acta*. 2009; **362**: 5-10.
47. Yoshida T, Kamato K, Tsukamoto M, Iida T, Schlettwein D, Wohrle D and Kaneko M. *J. Electroanal. Chem.* 1995; **385**: 209-225.
48. Abe T, Yoshida T, Tokita S, Taguchi F, Imaya H and Kaneko M. *J. Electroanal. Chem.* 1996; **412**: 125-132.
49. Zhang AJ, Zhang WM, Lu JX, Wallace GG and Chen J. *Electrochem. Solid State Lett.* 2009; **12**: E17-E19.
50. Isaacs M, Armijo F, Ramirez G, Trollund E, Biaggio SR, Costamagna J and Aguirre MJ. *J. Mol. Catal. A: Chem.* 2005; **229**: 249-257.
51. Quezada D, Honores J, Garcia M, Armijo F and Isaacs M. *New. J. Chem.* 2014; **38**: 3606-3612.
52. Yao SA, Ruther RE, Zhang LH, Franking RA, Hamers RJ and Berry JF. *J. Am. Chem. Soc.* 2012; **134**: 15632-15635.

53. Hiratsuka K, Takahashi K, Sasaki H and Toshima S. *Chem. Lett.* 1977: 1137-1140.
54. Takahashi K, Hiratsuka K, Sasaki H and Toshima S. *Chem. Lett.* 1979: 305-308.
55. Enoki O, Imaoka T and Yamamoto K. *Macromol. Symp.* 2003; **204**: 151-158.
56. Imaoka T, Nakazawa S and Yamamoto K. *Chem. Lett.* 2001: 412-413.
57. Imaoka T, Tanaka R and Yamamoto K. *J. Polm. Sci., Part A: Polym. Chem.* 2006; **44**: 5229-5236.
58. Hammouche M, Lexa D, Saveant JM and Momenteau M. *J. Electroanal. Chem.* 1988; **249**: 347-351.
59. Costentin C, Passard G, Robert M and Saveant JM. *J. Am. Chem. Soc.* 2014; **136**: 11821-11829.
60. Lexa D, Saveant JM, Su KB and Wang DL. *J. Am. Chem. Soc.* 1988; **110**: 7617-7625.
61. Lexa D, Saveant JM, Schafer HJ, Su KB, Vering B and Wang DL. *J. Am. Chem. Soc.* 1990; **112**: 6162-6177.
62. Anxolabehere E, Chottard G and Lexa D. *New. J. Chem.* 1994; **18**: 889-899.
63. Hammouche M, Lexa D, Momenteau M and Saveant JM. *J. Am. Chem. Soc.* 1991; **113**: 8455-8466.
64. Bhugun I, Lexa D and Saveant JM. *J. Phys. Chem.* 1996; **100**: 19981-19985.
65. Bhugun I, Lexa D and Saveant JM. *J. Am. Chem. Soc.* 1994; **116**: 5015-5016.
66. Bhugun I, Lexa D and Saveant JM. *J. Am. Chem. Soc.* 1996; **118**: 1769-1776.
67. Costentin C, Drouet S, Passard G, Robert M and Saveant JM. *J. Am. Chem. Soc.* 2013; **135**: 9023-9031.
68. Costentin C, Drouet S, Robert M and Saveant JM. *Science*. 2012; **338**: 90-94.
69. Rakowski DuBois M and DuBois DL. *Chem. Soc. Rev.* 2009; **38**: 62-72.
70. Hull JF, Himeda Y, Wang WH, Hashiguchi B, Periana R, Szalda DJ, Muckerman JT and Fujita E. *Nature Chemistry*. 2012; **4**: 383-388.
71. Fujita E, Muckerman JT and Himeda Y. *Biochim. Biophys. Acta-Bioenerg.* 2013; **1827**: 1031-1038.
72. Grodkowski J, Behar D, Neta P and Hambright P. *J. Phys. Chem. A.* 1997; **101**: 248-254.
73. Hoshino M, Ueda K, Takahashi M, Yamaji M, Hama Y and Miyazaki Y. *J. Phys. Chem.* 1992; **96**: 8863-8870.
74. Behar D, Dhanasekaran T, Neta P, Hosten CM, Ejeh D, Hambright P and Fujita E. *J. Phys. Chem. A.* 1998; **102**: 2870-2877.
75. Neta P. *J. Phys. Chem.* 1981; **85**: 3678-3684.
76. Baral S, Neta P and Hambright P. *Radiat. Phys. Chem.* 1984; **24**: 245-255.
77. Baral S, Hambright P and Neta P. *J. Phys. Chem.* 1984; **88**: 1595-1600.
78. Qiu AM and Sawyer DT. *J. Porphyrins and Phthalocyanines*. 1997; **1**: 125-134.
79. Dhanasekaran T, Grodkowski J, Neta P, Hambright P and Fujita E. *J. Phys. Chem. A.* 1999; **103**: 7742-7748.
80. Matsuoka S, Kohzuki T, Pac C, Ishida A, Takamuku S, Kusaba M, Nakashima N and Yanagida S. *J. Phys. Chem.* 1992; **96**: 4437-4442.
81. Grodkowski J and Neta P. *J. Phys. Chem. A.* 2000; **104**: 1848-1853.
82. Grodkowski J, Dhanasekaran T, Neta P, Hambright P, Brunschwig BS, Shinozaki K and Fujita E. *J. Phys. Chem. A.* 2000; **104**: 11332-11339.
83. Grodkowski J, Neta P, Fujita E, Mahammed A, Simkhovich L and Gross Z. *J. Phys. Chem. A.* 2002; **106**: 4772-4778.
84. Fujita E, Creutz C, Sutin N and Szalda DJ. *J. Am. Chem. Soc.* 1991; **113**: 343-353.

Table 1. Electrocatalytic CO_2 reduction using catalysts non-covalently adsorbed onto electrodes.

	Complex	electrode	Product (FE) / TON or TOF	Catalytic species	E/V
1	CoPc [a]	Dip-coated from benzene on graphite	oxalic acid, glycolic acid, but no formate	$[Co(Pc^{\bullet-})]^{2-}$	–1.6 (SCE)
2	CoPc [b]	Precipitated from sulfuric acid with water on glassy carbon	formate (60) methanol(5)	---	–1.2 to –1.4 (SCE)
3	CoPc [c]	Dip coated or drop cast from THF on glassy carbon	formate (55-60) / TON = 3.7×10^5 H_2 (35-30)	$[CoPcH]^{-}$ [1]	–1.15 (SSCE)
4	CoPc [d]	Plasma assisted vacuum deposition on glassy carbon	---	---	–1.6 (SSCE)
5	$CuPc(OBu)_8$ [e]	Drop cast from DMF on basal plain pyrolytic graphite	CO/H_2 ~4.2 / TOF = 1.1×10^6 h^{-1}	$[CoPcH]^{-}$ [1]	–1.3 (Ag/AgCl)
6	CoPc [f]	Gas diffusion electrode on carbon black with PTFE	CO (100) H_2 (14)	$[Co^{I}(Pc^{\bullet-})]^{2-}$	–1.5 (SCE)
7	CoPc [g]	Gas diffusion electrode on carbon black with PTFE	CO (100)	$[CoPc]^{2-}$	–1 to –1.75 (NHE)
8	FePc [g]	Gas diffusion electrode on carbon black with PTFE	CO (80)	$[FePc]^{2-}$	–1.5 (NHE)
9	CoTPP [h] FeTPP [h]	Gas diffusion electrode on carbon black with PTFE	CO (97) CO (85)	$[Co^{I}TPP]^{-}$ [m] $[Fe^{I}TPP]^{-}$ [m]	−0.96 –1.01 (Ag/AgCl)
10	CoTMPP [i]	Activated carbon fiber, dip coated	CO (70)		–1.3 (SCE)
11	Co(tmtppa) [j]	Dip cast on graphite disc, protected with Nafion	---	$[Co^{I}(Pc^{\bullet-})]^{2-}$	–1.1 (SCE)
12	CoTAPc [k]	MWCNT/Co composite, layer by layer	formate (78)	---	–0.5 (Ag/AgCl)

[a] Reference [15], 0.05M Et_4NClO_4. [b] Reference [16], bicarbonate pH 3-7. [c] Reference [17], 0.05M citrate, pH 5. [d] Reference [19], 0.5 M Na_2SO_4/HCO_3^- pH 6.65. [e] Reference [20], pH 4. [f] Reference [23], sodium sulfate pH 2. [g] Reference [24], 0.5 M bicarbonate pH 7.6. [h] Reference [26], 0.5 M $KHCO_3$. [i] Reference [27], 0.5M $KHCO_3$. [j] Reference [28], Britton-Robinson buffer pH 5.5. [k] Reference [30], 0.1 M $KHCO_3$. [l] While $[CoPcH]^-$ means a protonated $[Co^{I}(Pc^{\bullet-})]^{2-}$ species, it is not clear the species is $[H–Co(Pc)]^-$ or $[Co(PcH)]^-$ from the original literature. [m] High pressure CO_2.

Table 2. Electrocatalytic CO_2 reduction using catalysts covalently bound to electrodes.

	Complex	electrode	Product (FE) / TON of TOF	Catalytic species	E/V
1	CoTPP	4-aminopyridine amide linked to glassy carbon	CO (>50) / TON 10^5	$[Co^I(tpp)(py)]^-$	–1.2 (SCE)
2	CoTPP	4-aminopyridine amide linked to glassy carbon	CO (92) / TON 10^7	$[Co^I(tpp)(py)]^-$	–1.1 (SCE)
3	CoTPP	4-aminopyriidne amide linked to glassy carbon	CO (45)	$[Co^I(tpp)(py)]^-$ with H^+ and CO_2	–1.3 (SCE)
4	CoTPP	Aminopyridine radical bound to glassy carbon	CO (60)	[H–Co(TPP)]	–1.1 (SCE)
5	Co(benzoPor)	4-aminopyridine radical bound to glassy carbon	--		–1.6 (Ag/AgCl)
6	CoPc	Poly-4-vinylpyridine on graphite	CO (69) H_2 (20) TOF 6.12×10^5	$[Co^I(PcH)]^-$ [1]	–1.5 (SCE)
7	CoPc	Poly-4-vinylpyridine on graphite			–1.2 (Ag/AgCl)
8	CoPc	Neat coating on graphite	$CO/H_2 = 6$	$[Co^I(PcH)]^-$ [1]	–1.2 (Ag/AgCl)
9	CoPc	Polypyrrole on glassy carbon, Co drop cast from THF	formate (72)	$[Co^IPc]$ with $H_{adsorbed}$	–1 (Ag/AgCl)
10	CoTAPc	Electropolymerized on glassy carbon	Formate / TOF 7.9×10^4 h^{-1}	Further reduced species of $[Co^I(TAPc^{\bullet-})]^{2-}$	–1 (Ag/AgCl)
12	CoTAPP	Electropolymerized on ITO	CO (65) / TON 69 Ionic liquid	$[Co^ITAPP]^-$	–0.8 (Ag/AgCl)
11	$CoTPC(CC)_3$	Click reaction on modified boron-doped diamond	CO / TOF 0.8 s^{-1}		–1.55 (Ag/AgCl)

[a] Reference [41], phosphate pH 6.86. [b] Reference [42], phosphate, pH 6.0. [c] Reference [43], phosphate pH 6.3. [d] Reference [44], phosphate pH 6.8. [e] Reference [46], phosphate pH 6.3 - 6.8. [f] Reference [47], phosphate pH 6.8. [g] Reference [48], phosphate pH 5. [h] Reference [49], $LiCLO_4$, CH_3CN/H_2O. [i] Reference [50], $NaClO_4$. [j] Reference [51], $BMImBF_4$. [k] Reference [52], CH_3CN, Bu_4NPF_6. [l] $[Co^I(PcH)]^-$ is the doubly reduced and the protonated ligand species formed from $[Co^{II}(Pc)]$.

Table 3. Photocatalytic CO_2 reduction.

Complex	Product	TON	Additives	Oxidation state	Solvent
FeTPP [a]	CO	70			DMF, 5% Et_3N
Fe-oTMPyP [a]	CO	~70		Fe(0)	Water, 5% Et_3N
CoTPP [b]	CO	300		Co(0)	DMF, 5% Et_3N
CoTmFP [b]	CO	~150		Co(0)	DMF, 5% Et_3N
CoTM(CF_3)PP [b]	CO	~150		Co(0)	DMF, 5% Et_3N
FeTPP [c]	CO	230	TP 3 mM	Fe(0)	DMF, 5% Et_3N
cobinamide [d]	CO	60	TP 3 mM	Co(0)	9:1 MeCN/MeOH, 5% Et_3N
Co(TBPc) [e]	CO	50	TP 3 mM	Co(I)$Pc^{\bullet-}$	DMF, 5% Et_3N
Co(tpfc) [f]	CO	100	TP 3 mM	Co(I)	MeCN, Et_3N (5%)
	H_2	60			
Fe(tpfc) [f]	CO	100	TP 3 mM	Fe(I)	MeCN, Et_3N (5%)
	H_2	190			

[a] Reference [72]. [b] Reference [74]. [c] Reference [79]. [d] Reference [81]. [e] Reference [82]. [f] Reference [83].

Table 4. Select reactions relevant to photocatalytic CO_2 reduction and mechanistic studies.

	Reaction	rate
1 [a]	$[ClFe^{III}P] + Et_3N \rightarrow Fe^{II}P + Cl^- + Et_3N^{\bullet+}$	
2 [a]	$Fe^{II}P + Et_3N \rightarrow [Fe^{I}P]^- + Et_3N^{\bullet+}$	
3 [a]	$[ClFe^{III}\text{-}oTMPyP] + Et_3N \rightarrow Fe^{II}\text{-}oTMPyPH_2 + Cl^- + Et_3N^{\bullet+}$	
4 [a]	$Fe^{II}\text{-}oTMPyP + e_{aq}^- \rightarrow [Fe^{I}\text{-}oTMPyP]^-$ $Fe^{II}\text{-}oTMPyP + CO_2^{\bullet-} \rightarrow [Fe^{I}\text{-}oTMPyP]^-$	
5 [a]	$2[Fe^{I}\text{-}oTMPyP]^- \rightarrow Fe^{II}P + [Fe^{0}P]^{2-}$	$(1.5 \pm 0.5) \times 10^8\ M^{-1}.s^{-1}$
6 [b]	$Co^{II}Por + e_{aq}^- \rightarrow [Co^{I}Por]^-$ $Co^{II}Por + CO_2^{\bullet-} \rightarrow [Co^{I}Por]^- + CO_2$	
7 [b]	$[Co^{I}TPPS]^- + e_{aq}^- \rightarrow [Co^{0}TPPS]^{2-}$ $[Co^{I}\text{-}mTMPyP]^- + e_{aq}^- \rightarrow [Co^{0}\text{-}mTMPyP]^{2-}$	$(2.1 \pm 0.4) \times 10^{10}\ M^{-1}.s^{-1}$ $(4 \pm 1) \times 10^{10}\ M^{-1}.s^{-1}$
8 [b]	$[Co^{I}\text{-}mTMPyP]^- + CO_2^{\bullet-} \rightarrow [Co^{0}\text{-}mTMPyP]^{2-} + CO_2$	$5 \times 10^9\ M^{-1}.s^{-1}$
9 [b]	$[Co^{I}TPPS]^- + e_{aq}^- \rightarrow$ chlorin, phlorin anion	
10 [c]	$M^{II}Por + TP^{\bullet-} \rightarrow [M^{I}Por]^- + TP$ $[M^{I}Por]^- + TP^{\bullet-} \rightarrow [M^{0}Por]^{2-}$	
11 [c]	$Co^{II}TPP + TP^{\bullet-} \rightarrow [Co^{I}Por]^- + TP$	$(1.0 \pm 0.2) \times 10^{10}\ M^{-1}.s^{-1}$
12 [c]	$Co^{I}TPP + TP^{\bullet-} \rightarrow [Co^{0}Por]^- + TP$	$(7 \pm 2) \times 10^9\ M^{-1}.s^{-1}$
13 [d]	$[Co^{I}B_{12}]^- + CO_2^{\bullet-} \rightarrow [(CO_2)CoB_{12}]^{2-}$	$(1.2 \pm 0.3) \times 10^8\ M^{-1}.s^{-1}$
14 [d]	$[Co^{I}B_{12}]^- + e_{aq}^- \rightarrow [Co^{0}B_{12}]^{2-}$	$1 \times 10^{10}\ M^{-1}.s^{-1}$
15 [e]	$Co^{II}TSPc + e_{aq}^- \rightarrow [Co^{I}TSPc]^-$ $Co^{II}TSPc + CO_2^{\bullet-} \rightarrow [Co^{I}TSPc]^- + CO_2$	
16 [e]	$Co^{II}TSPc + e_{aq}^- \rightarrow [Co^{I}TSPc]^-$	$2 \times 10^{10}\ M^{-1}.s^{-1}$
17 [e]	$[Co^{I}TSPc]^- + CO_2^{\bullet-} \rightarrow [Co^{I}TSPcCO_2]^{2-}$	$5.5 \pm 0.8 \times 10^7\ M^{-1}.s^{-1}$
18 [e]	$Co^{II}TSPc + TP^{\bullet-} \rightarrow [Co^{I}TSPc]^-$	
19 [e]	$Co^{II}Pc + TP^{\bullet-} \rightarrow [Co^{I}Pc]^- + TP$ $Co^{I}Pc + TP^{\bullet-} \rightarrow [Co^{0}Pc]^- + TP$	$2 \times 10^{10}\ M^{-1}.s^{-1}$ $(7.8 \pm 1.2) \times 10^9\ M^{-1}.s^{-1}$

[a] Reference [72]. [b] Reference [74]. [c] Reference [79]. [d] Reference [81]. [e] Reference [82].